ADVANCES IN ATMOSPHERIC SCIENCES, VOL. 43, MAY 2026, 1033–1047

• **Original Paper** •

Mobile Observations of Intracity Variations in Atmospheric CO_2 and CH_4

Jun WANG[1], Wei XIAO*[1], Ning HU[2], Ruonan LI[2], Honghui XU[3], Yibo LIU[1], Lingbing BU[2], Longlong CHEN[1], Yuanze LIU[1], and Xuhui LEE[4]

[1]*Key Laboratory of Ecosystem Carbon Source and Sink-China Meteorological Administration (ECSS-CMA)*, *Nanjing University of Information Science & Technology*, *Nanjing* 210044, *China*

[2]*Yale-NUIST Center on Atmospheric Environment*, *Collaborative Innovation Center on Forecast and Evaluation of Meteorological Disasters*, *Nanjing University of Information Science & Technology*, *Nanjing* 210044, *China*

[3]*Zhejiang Lin'an Atmospheric Background National Observation and Research Station*, *Hangzhou* 310008, *China*

[4]*School of the Environment*, *Yale University*, *New Haven*, *Connecticut* 06511, *USA*

(Received 21 March 2025; revised 28 July 2025; accepted 1 September 2025)

ABSTRACT

The spatial variability in the atmospheric CO_2 and CH_4 concentrations in urban land is affected by the source type, source distribution, and emission intensity in the cityscape. In this study, we analyzed vehicle-mounted measurements of street-level CO_2 and CH_4 concentrations in Hangzhou—a large metropolitan area in the Yangtze River Delta in eastern China. The results revealed that CO_2 and CH_4 emission hotspots did not overlap geographically, with the former occurring as linear features at elevated road intersections and expressways and the latter occurring at waste treatment facilities (sewage treatment plants and landfills). The CH_4:CO_2 emission ratios (ppb ppm^{-1}) were ranked in increasing order as follows: traffic (1.01 ± 1.82; mean ± 1 SD); overall (3.46 ± 2.71); sewage treatment (12.76 ± 2.50); and landfill (36.50 ± 10.15). Waste treatment was largely responsible for the increased overall emission ratio, supporting this source category as a major contributor to the CH_4 budget in this city and suggesting a negligible role of domestic appliances (cookstoves and water heaters). A two-source mixing model calculation indicated that 99.9% of nonelectric vehicles in Hangzhou were gasoline-powered, revealing a recent shift in vehicle fuel composition from gasoline/natural gas to gasoline/electricity. The methodology established in this study is applicable to cities elsewhere.

Key words: CH_4 and CO_2, vehicle-mounted observations, emission hotspots, CH_4:CO_2 emissions ratio, emission source composition

Citation: Wang, J., and Coauthors, 2026: Mobile observations of intracity variations in atmospheric CO_2 and CH_4. *Adv. Atmos. Sci.*, **43**(5), 1033–1047, https://doi.org/10.1007/s00376-025-5059-4.

Article Highlights:

- Citywide atmospheric CO_2 and CH_4 measurements across the day, night, and season in Hangzhou.
- CO_2 and CH_4 emission hotspots did not overlap.
- Waste treatment was responsible for elevated CH_4 concentrations in the city.
- A total of 99.9% of nonelectric vehicles were gasoline-powered.

1. Introduction

Cities are large sources of anthropogenic greenhouse gases (GHGs). Cities account for more than 70% of global CO_2 emissions and 15%–40% of CH_4 emissions despite their comprising less than 2.4% of the Earth's land area (Potere and Schneider, 2007; Duren and Miller, 2012; Seto et al., 2014). Researchers commonly estimate GHG emissions using "top-down" and "bottom-up" methods. The top-down approach estimates CH_4 and CO_2 emissions by combining GHG concentration data with atmospheric transport models (Ciais et al., 2010; Turner et al., 2016; Lopez-Coto et al., 2017; Wu et al., 2018; Cui et al., 2019; Huang et al., 2021). Because these models rely on sparse monitoring stations, they can only produce emission estimates at the regional scale. In principle, the approach can be extended to estimate emissions in cities. A prerequisite for the successful applica-

* Corresponding author: Wei XIAO
Email: wei.xiao@nuist.edu.cn

tion of city-scale top-down modeling is obtaining high spatial resolution, near-surface atmospheric CH_4 and CO_2 concentration data from the cityscape.

The bottom-up approach, or inventory method, has been shown to be accurate at national and regional scales (Oda et al., 2019; Mustafa et al., 2021), but it often produces large errors at urban scales (Marcotullio et al., 2014; Cai et al., 2019; Ahn et al., 2023). These errors are related to the inaccuracy of emission allocation schemes (Wang et al., 2013). Inventory products allocate total emissions to grid points on the basis of the spatial distributions and temporal variation characteristics of point sources (e.g., power plants), line sources (e.g., road networks), and surface sources (e.g., building energy use) (Janssens-Maenhout et al., 2019; Crippa et al., 2020; Chen et al., 2021). However, the lack of precise information on source distributions often results in unreasonable emission allocations (Han et al., 2020). Moreover, inventory products cannot fully capture the diurnal variation in emissions or determine emission hotspots in urban areas. Identifying emission hotspots is also needed to help urban communities prioritize their carbon mitigation efforts. Direct monitoring of GHG concentrations in urban areas can reveal information about emission hotspots and spatial distributions of emission sources and source types.

Observational data, if they achieve high accuracy and are replicated densely across space, may aid top-down inverse modeling in constraining urban emission estimates. Typically, urban GHG monitoring is achieved with networks of surface stations or ground-based column observations (e.g., Turner et al., 2016). However, these approaches are expensive and often unable to meet the requirements of high spatial resolution. Vehicle-mounted mobile observation is a potential alternative for collecting high-resolution data in urban environments (Shorter et al., 1996; Bush et al., 2015; Lee et al., 2017; Weller et al., 2018; Wei and Wang, 2020; Joo et al., 2024). Previous studies have investigated the spatiotemporal characteristics of GHGs in Chinese megacities such as Beijing and Shanghai. However, these investigations have focused primarily on urban–rural contrasts or seasonal variations (Sun et al., 2019; Wei and Wang, 2020; Liu et al., 2021), whereas diurnal variations—particularly after 2000 Local Standard time (LST, LST=UTC+8)—remain relatively underexplored.

If multiple gas species are monitored simultaneously, the compositions of GHG sources can be disentangled. Xueref-Remy et al. (2011) reported that the multigas ratio method is useful for identifying emission types. This method is based on the assumption that the emission sources of the target gas (e.g., CH_4) and the tracer gas (e.g., CO_2) are colocated and experience the same atmospheric transport, dispersion, and dilution processes. In the absence of additional external emission sources, the ratio of the two gases should be constant. Another key assumption is that the two gases do not undergo significant chemical reactions over short time scales and that their concentration changes are controlled solely by emission and diffusion processes (Hsu et al., 2010). This method is currently widely applied in research on the basis of concentration observations. For example, researchers have used the C_2H_6:CH_4 ratio to differentiate between biological sources and anthropogenic sources (Joo et al., 2024). Similarly, the CH_4:CO_2, CO:CO_2, and CH_4:CO ratios have been used to trace and identify emission source types (Hu et al., 2018; Sun et al., 2019; Li et al., 2022).

In this study, we employed vehicle-mounted instruments to measure the near-surface CO_2 and CH_4 concentrations in Hangzhou city in the Yangtze River Delta, China. The urban land of Hangzhou is relatively compact and consists of multiple functional areas and emission hotspots. Disentangling their roles in the urban GHG budget requires repeated and balanced sampling in space and time. Vehicles are among the major sources of both CO_2 and CH_4 emissions in urban areas (Nakagawa et al., 2005; Hu et al., 2018; Clairotte et al., 2020; Pan et al., 2020; Wei and Wang, 2020). Previous studies have shown that vehicle exhaust, especially from natural gas vehicles, can contribute significantly to CH_4 emissions, with emission factors varying according to fuel type, combustion efficiency, and operating conditions. Like other cities in the region, Hangzhou has recently experienced rapid changes in vehicle fuel composition, transitioning from gasoline to natural gas and then to electricity. However, the extent to which this energy transition affects ambient CO_2 and CH_4 concentrations is not known. Unlike previous studies in megacities (Wei and Wang, 2020; Liu et al., 2021), our measurements were conducted at multiple times of the day and in multiple seasons to develop a robust framework for mapping emission hotspots.

The objectives of this study were to (1) characterize the spatiotemporal distributions of CO_2 and CH_4 concentrations, (2) identify emission hotspots, and (3) determine the composition of emission sources in various functional areas, including an assessment of vehicle fuel composition changes. Our study appears to be the first to conduct comprehensive measurements of both CO_2 and CH_4 across a large city in the daytime and nighttime and in all seasons.

2. Materials and methods

2.1. *Study area and observation method*

The field campaign was conducted in Hangzhou (29°11′N–30°34′N, 118°20′E–120°37′E; Fig. 1)—a city in the Yangtze River Delta, in eastern China. Hangzhou encompasses an area of 16 850 km^2 and has a population of approximately 12 million. Hangzhou experiences a subtropical monsoon climate and includes various functional areas, such as industrial areas, commercial–residential mixed areas, natural scenic landscapes, and riverside residential districts.

Near-surface atmospheric CO_2 and CH_4 concentrations were monitored using vehicle-mounted analyzers from the winter of 2020 to the autumn of 2023 (Fig. 1 and Table 1). More detailed information is provided in section 1.1 of the electronic supplementary material (ESM).

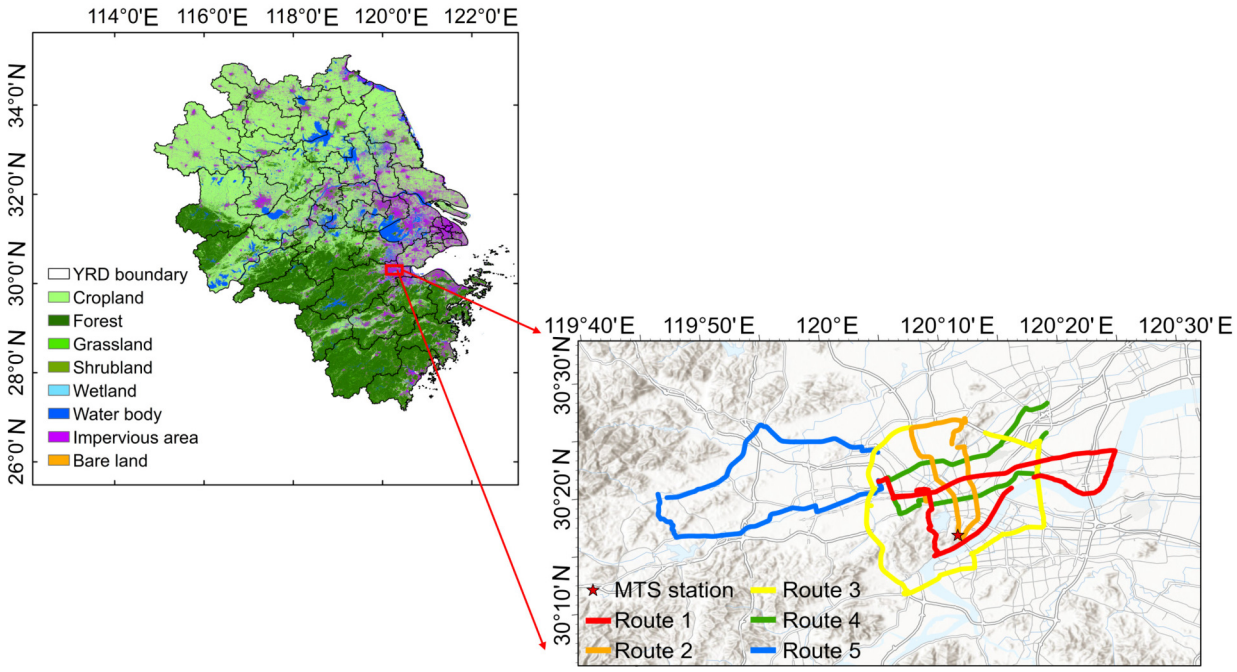

Fig. 1. Land use types in the Yangtze River Delta (left-hand panel; data source: Gong et al., 2019) and observation routes in Hangzhou (right-hand panel).

Table 1. Observation periods and routes.

Year	Season	Date	Period (LST)	Routes
2020	Winter	26, 27 December	0830–1230 2030–2330	1, 2, 3, 4
2021	Spring	15, 17 April	0930–1230 2130–2400	1, 2, 4, 5
2021	Autumn	28, 30 October	0930–1230 2130–2400	1, 2, 4, 5
2022	Winter	8, 10, 11 January	0930–1230 2130–2400	1, 2, 4, 5
2022	Summer	28, 30 July	0930–1230 1400–1800 2130–2400	1, 2, 4, 5
2023	Summer	11–13 August	0930–1200 1400–1630 2000–2230	1, 2, 3, 4
2023	Autumn	25–27 September 30, 31 October 1 November	0930–1200 1400–1630 2000–2230	1, 2, 3, 4

Each campaign employed four portable CO_2/CH_4/H_2O analyzers based on off-axis integrated cavity output spectroscopy (Model 915-0011, Los Gatos Research, Mountain View, CA, USA). These instruments measured CO_2 and CH_4 concentrations in the near-ground urban atmosphere with a sampling frequency of 1 Hz. The measurement accuracies were as follows: CH_4 < 2 ppb, CO_2 < 0.3 ppm, and H_2O < 100 ppm. The details of the calibration are provided in section 1.2 of the ESM. A Teflon tube equipped with a filter and an inverted funnel at the air inlet was used as the sampling line to prevent the entry of insects, particles, and rainwater. The air inlet, located approximately 2.5 m above the ground on top of the vehicle, extended from the roof. The sampling lag time, caused by the length of the tube, was calculated from the instrument flow rate and the length and diameter of the tube. This lag time was corrected during data processing. Data were excluded if the vehicle speed was less than 10 km h^{-1} to minimize the effect of vehicular exhaust at low speeds. A GPS and a video recorder were used to document latitude, longitude, and traffic conditions with a sampling frequency of 1 Hz.

Data on background CO_2 and CH_4 concentrations were obtained from the Hangzhou National Reference Climate Station, located at Mantoushan Mountain in central Hangzhou (MTS station, 30.2294°N, 120.1760°E, 43.2 m above sea level; marked as a star in Fig. 1). This station uses a CO_2/CH_4/H_2O analyzer based on cavity ring-down spectroscopy (Model G2301, Picarro Inc., Santa Clara, CA,

USA) to continuously monitor atmospheric concentrations. The station is situated on a hill in Hangzhou, with no nearby buildings that can obstruct airflow. The intake is mounted atop a tower, approximately 45 m above the main open streets of Hangzhou—this elevation is the combined height of the tower and the hill (Fang et al., 2022). The concentration footprint of the station encompasses mainly urban built-up land (Hu et al., 2023), making it representative of background concentration variations within the city. The instrument was calibrated with a linear two-point method using two standard gases with high and low concentrations. A target gas with known concentrations was analyzed every six hours to calibrate the system. All standards were traceable to the WMO X2007 scale (Zhao and Tans, 2006), and the gases were pressurized in aluminum cylinders (Fang et al., 2022). More detailed information about the station is provided in Zhang et al. (2024) and Qi et al. (2025).

2.2. *Data processing*

2.2.1. *Tunnel data*

In traffic tunnels, where numerous vehicles are present and diffusion conditions are poor, CH_4 and CO_2 concentrations tend to accumulate and reach high levels. Since tunnels are not affected by external sources, the data collected inside them were used directly for analysis of vehicle emissions. In this study, ten tunnels were measured a total of 274 times. The length of each tunnel pass-through ranged from 1 min to 5 min. The CH_4:CO_2 emissions ratio was obtained by geometric regression, with each sample representing a 1 s observation. An example is presented in Fig. S1 in the ESM.

Traffic tunnels are enclosed environments affected only by vehicle emissions, making them useful for identifying the proportion of gasoline-powered vehicles versus natural gas-powered vehicles in a city. A two-source mixing model was used to calculate the percentage of gasoline vehicles, using the emissions ratio obtained for the tunnels, as follows:

$$P_{gv} = \frac{R_{tunnel} - R_{ngv}}{R_{gv} - R_{ngv}}, \quad (1)$$

where R_{gv} represents the emissions ratio for gasoline vehicles, the value of which was obtained from the IPCC (Stocker et al., 2013). R_{ngv} denotes the emissions ratio for natural gas vehicles, and the value was obtained from Hu et al. (2018). R_{tunnel} indicates the emissions ratio obtained for the tunnels, and P_{gv} represents the percentage of gasoline vehicles.

2.2.2. *Open street data*

To account for the temporal variability of background concentrations during mobile sampling, the difference between the street-level concentration (C_{obs}) and the urban reference concentration (C_{ref}) measured at the same time was calculated ($\Delta = C_{obs} - C_{ref}$). These differences, denoted as ΔCH_4 and ΔCO_2, were used to represent the spatial patterns of near-surface CH_4 and CO_2 concentrations. The geometric regression method was used to calculate the CH_4:CO_2 emissions ratio on the basis of these differences. To reduce measurement noise, the data collected from open streets were averaged over 100 m segments. Each data sample in the regression represents the spatial average over a 100-m street segment. An example is presented in Fig. S2 in the ESM.

2.3. *Emission hotspots*

Emission hotspots were defined as locations with repeatedly high values of ΔCH_4 or ΔCO_2. For each observation, the top 10% of the ΔCH_4 and ΔCO_2 values along the four routes were classified as "high values". Locations with high values in more than half of the observations were categorized as stable hotspots. If high values were present in 33% to 50% of the observations, the location was defined as a moderately stable hotspot. Locations with high values in less than 33% of the observations were classified as unstable hotspots. To minimize random variations, locations had to be traversed at least four times to be considered for hotspot classification.

To analyze the nature of some emission hotspots, data within a 1000-m radius of a target source were selected. The area within a 300-m radius was defined as the "inner ring", representing the zone most directly affected by the source, whereas measurements in the 300–1000 m radius (the "outer ring") were less affected by the direct emissions from the source.

2.4. *Urban functional areas*

The vehicle observation routes consisted of various functional areas within Hangzhou. Definitions of these areas were based on two governmental documents (Hangzhou Bureau of Planning and Natural Resources, 2020; Hangzhou Bureau of Statistics, 2020). These areas included industrial areas (primarily around the Hangzhou Iron Plant), commercial–residential mixed areas (downtown), natural scenic areas (the West Lake area), and riverside residential areas (residential districts along the Qiantang River).

3. Results

3.1. *CH_4 and CO_2 Concentrations and Emission Ratios in Open Streets*

Figure 2 shows the probability distributions of the near-surface atmospheric CH_4 and CO_2 concentrations, the corresponding enhancements (ΔCH_4 and ΔCO_2), and the CH_4 and CO_2 concentrations at the MTS reference station during the observation periods. During the day, the CH_4 concentration ranged from 1870 to 3478 ppb, with a median value of 2193 ppb. At night, the concentration varied from 1970 to 6787 ppb, with a median value of 2288 ppb. The median CH_4 concentration was 95 ppb higher at night than during the day. In terms of enhancement, ΔCH_4 during the day ranged from −395 to 1335 ppb, with a median value of 10

ppb. At night, ΔCH_4 ranged from −351 to 4372 ppb, with a median value of 57 ppb. At the reference station, the CH_4 concentration during the day ranged from 2006 to 2606 ppb, with a median value of 2200 ppb. At night, the CH_4 concentration ranged from 2090 to 2557 ppb, with a median value of 2272 ppb.

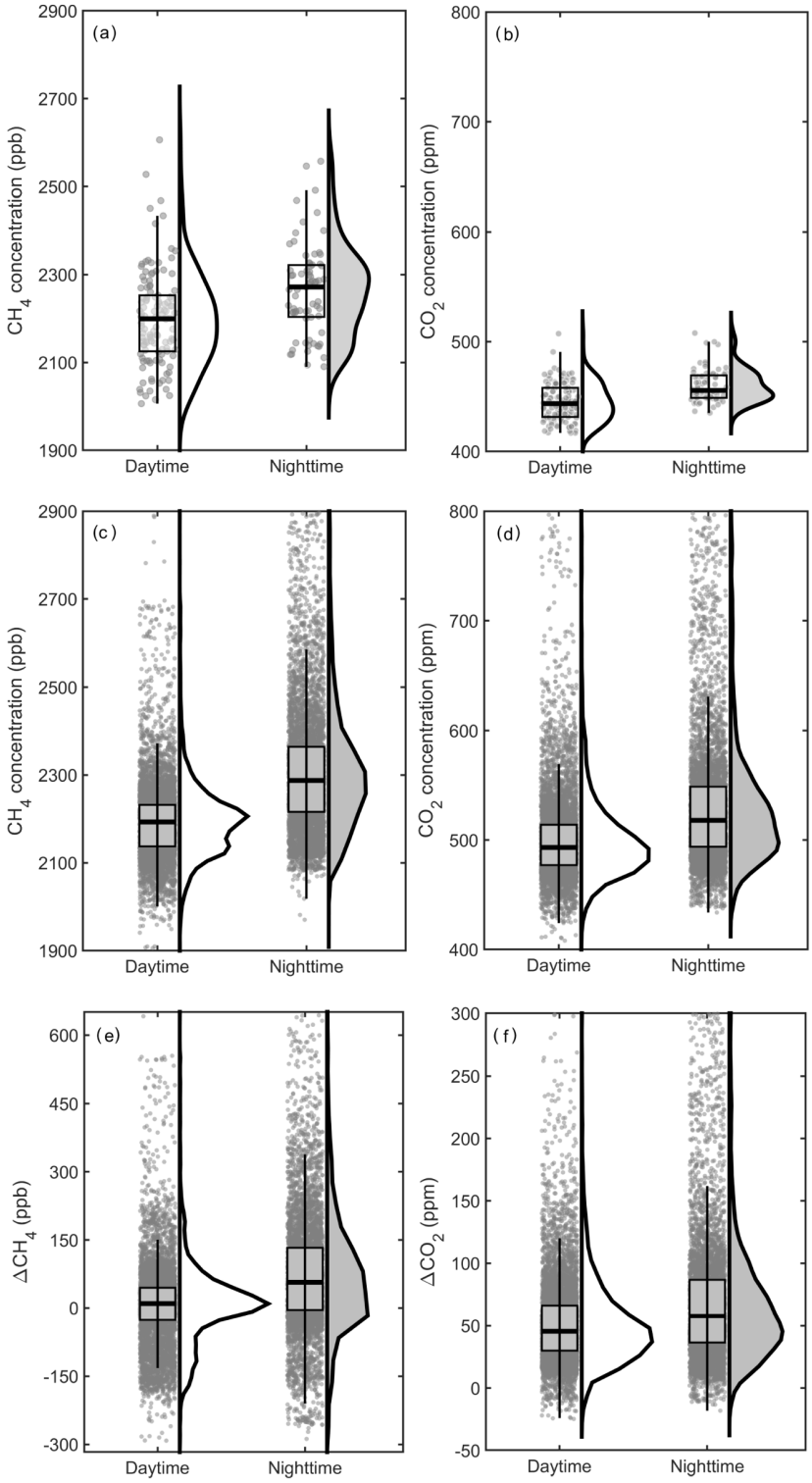

Fig. 2. Variations in CH_4 and CO_2 concentrations at the MTS reference station (a and b; hourly averages), near-surface atmospheric CH_4 and CO_2 concentrations (c and d), and ΔCH_4 and ΔCO_2 (e and f) in open streets, showing the median (lines), 25th and 75th percentiles (boxes), 5th and 95th percentiles (whiskers), and frequency distributions (curves).

Similar diurnal variability was detected for the CO_2 concentration. During the day, the CO_2 concentration ranged from 408.1 to 1464.0 ppm, with a median concentration of 493.2 ppm. At night, the CO_2 concentration ranged from 433.7 to 1097.2 ppm, with a median concentration of 518.0 ppm. The median CO_2 concentration was 24.8 ppm higher at night than during the day. The corresponding ΔCO_2 values ranged from −24.7 to 1023.4 ppm during the day, with a median value of 45.5 ppm, and from −18.1 to 629.8 ppm at night, with a median value of 57.4 ppm. Compared with the median ΔCO_2 during the day, the median ΔCO_2 at night increased by 11.9 ppm. At the reference station, the CO_2 concentration ranged from 416.8 to 507.3 ppm during the day, with a median concentration of 443.5 ppm. At night, the CO_2 concentration ranged from 435.1 to 507.9 ppm, with a median concentration of 455.6 ppm.

Figure 3 presents the probability distribution of the ΔCH_4:ΔCO_2 emission ratio according to 110 daytime observations and 75 nighttime observations. Each data point represents one trip in one route, which was calculated as the slope of the geometric regression of the two concentration enhancements. The daytime ratio ranged from −7.21 to 26.36 ppb ppm^{-1}, with a median ratio of 2.43 ppb ppm^{-1}. At night, the daytime ratio ranged from −12.00 to 28.24 ppb ppm^{-1}, with a median ratio of 4.60 ppb ppm^{-1}. The nighttime median was much greater than the daytime median, with an increase of 2.17 ppb ppm^{-1}. By combining daytime and nighttime emission ratio data and removing the top 5% and bottom 5% of extreme values, we obtained an overall mean of 3.46 ppb ppm^{-1} and a standard deviation of 2.71 ppb ppm^{-1}.

The concentrations and enhancements of these gases exhibit seasonal variations (Fig. S3 in the ESM). The seasonal median CH_4 concentration exhibited the following trend: winter (2262 ppb) > autumn (2242 ppb) > spring (2210 ppb) > summer (2194 ppb). The CH_4 enhancement was greater in the spring (50 ppb) and the winter (49 ppb) and lower in the summer (4 ppb) and the autumn (20 ppb). In terms of CO_2, the seasonal median concentration showed in the following order: winter (533.5 ppm) > spring (510.4 ppm) > autumn (491.6 ppm) > summer (475.2 ppm). Similar to the changes in ΔCH_4, ΔCO_2 had a higher median in the spring (65.5 ppm) and the winter (67.2 ppm) and a lower median in the summer (36.7 ppm) and the autumn (39.2 ppm).

The emissions ratio had a slightly higher median value in the summer (3.26 ppb ppm^{-1}) and the autumn (3.04 ppb ppm^{-1}) than in the spring (2.82 ppb ppm^{-1}) and the winter (2.84 ppb ppm^{-1}; Fig. S4 in the ESM). The seasonal variation (~15%) was smaller than the day-versus-night variation (~75%).

3.2. *Emission hotspots*

The location and number of emission hotspots exhibited notable temporal variability, with hotspots scattered throughout the city (Fig. 4). During the day, two stable CH_4 emission hotspots were identified, both of which were located at road intersections with elevated bridges. Six moderately stable hotspots were identified at a sewage plant, a landfill site, three elevated bridges, and a residential area. At night, the locations of emission hotspots shifted, and the stability of these sources also changed. The number of stable emission sources increased to six, with the sewage plant, the landfill, elevated bridges, and residential areas becoming stable hotspots. Four additional moderately stable hotspots appeared at the intersections of large elevated bridges. Unstable hotspots, detected primarily on elevated roads, appeared in the form of small clusters.

The spatial distribution of CO_2 hotspots differed from that of CH_4 hotspots (Figs. 4c and d). Most CO_2 emission hotspots followed major roads and appeared as linear features. During the day, six stable hotspots were identified at elevated road intersections and expressways. Two moderately stable hotspots were located at a toll station and a shipping terminal. At night, the number of stable CO_2 hotspots

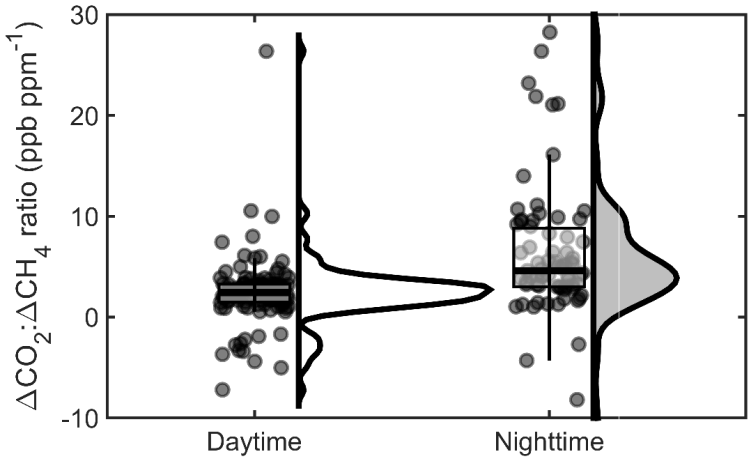

Fig. 3. Variations in the CH_4:CO_2 emissions ratio in open streets, showing the median (line), 25th and 75th percentiles (box), 5th and 95th percentiles (whisker), and frequency distribution (curve).

decreased to three, with those at the shipping terminal and main roads remaining. The number of moderately stable hotspots increased to four, with additional hotspots appearing at toll stations and along major roads. Unstable CO_2 hotspots were detected mainly along elevated roads and expressways with heavy traffic.

As urban infrastructure, sewage treatment plants and landfills are typical emission hotspots. Figure 5a shows the ΔCH_4 and ΔCO_2 correlations around the Qige Sewage Treatment Plant, which is located in the riverside residential area southeast of Route 1 (Fig. 1). The median ΔCH_4 and ΔCO_2 in the inner ring were 114 ppb and 28.6 ppm, respectively,

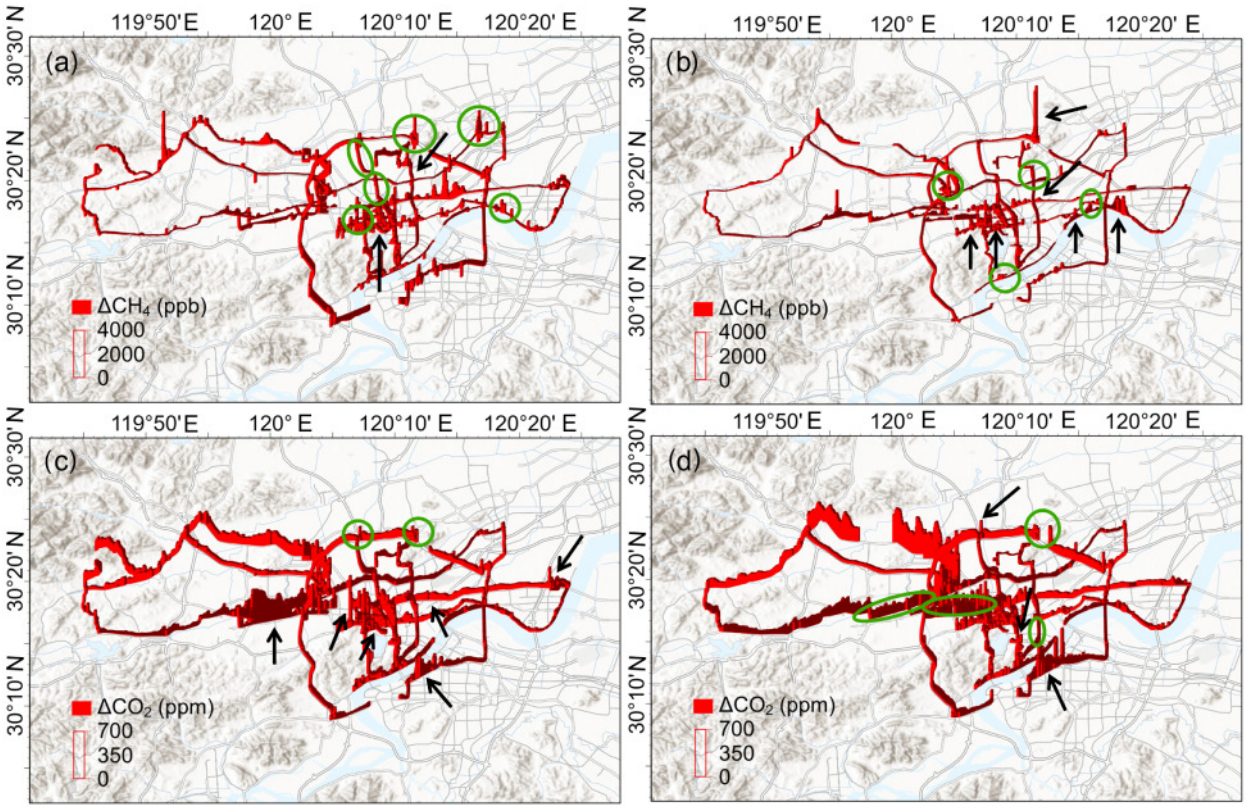

Fig. 4. Spatial patterns of the mean daytime and mean nighttime ΔCH_4 and ΔCO_2: (a) ΔCH_4 during the day; (b) ΔCH_4 at night; (c) ΔCO_2 during the day; (d) ΔCO_2 at night. Black arrows: stable hotspots; green circles: moderately stable hotspots.

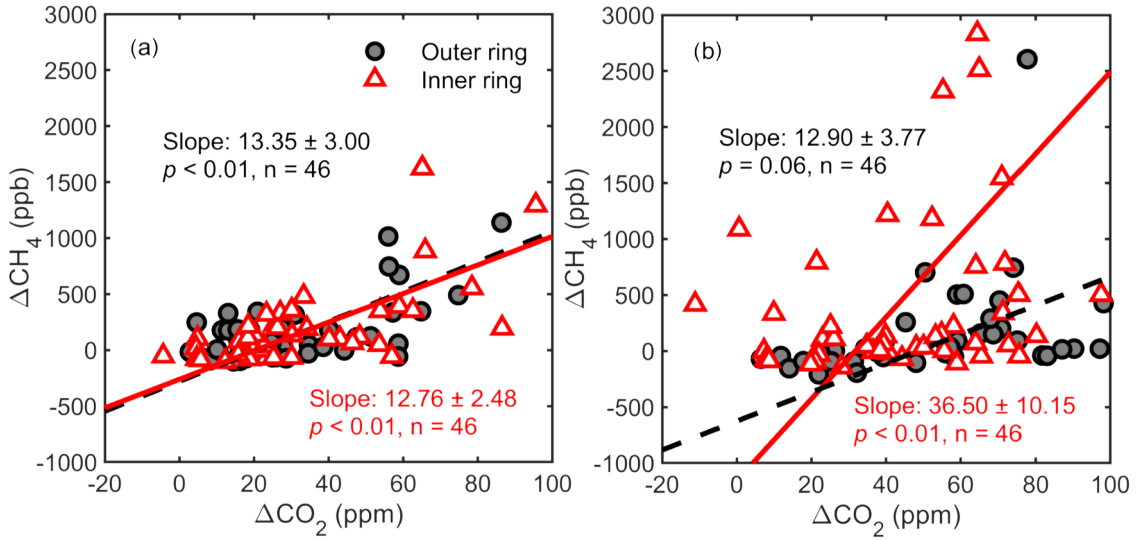

Fig. 5. Scatter plot of ΔCH_4 and ΔCO_2: (a) sewage treatment plant; (b) landfill. Observations in the inner ring are denoted by open triangles, and those in the outer ring are denoted by solid circles. Lines indicate linear regression with statistics noted (slope value ± 95% confidence bounds).

whereas in the outer ring, the median values were 64 ppb and 26.2 ppm, respectively. These values were much greater than the median values for open streets obtained in the four seasons across the whole city (Fig. 2). There was no significant difference in the ΔCH_4 or ΔCO_2 between the measurement locations within the inner ring and those within the outer ring ($p > 0.05$). The nearly identical emission ratios between the inner ring and the outer ring (13.35 ppb ppm^{-1} versus 12.76 ppb ppm^{-1}) suggest that the sewage treatment plant was the single source of emissions.

Figure 5b shows the ΔCH_4 and ΔCO_2 correlations near the Tianziling Landfill, located in northern Hangzhou, at the northeast corner of Route 2 (Fig. 1). This landfill was put into use in 1991 and was closed in 2020. In the inner ring, the median ΔCH_4 and ΔCO_2 values were 109 ppb and 46.2 ppm, respectively, and in the outer ring, the median ΔCH_4 and ΔCO_2 values were 21 ppb and 57.7 ppm, respectively. A significant difference was detected between the two regions for both gases ($p < 0.05$). The inner ring ratio was 36.50 ppb ppm^{-1}, whereas the outer ring ratio decreased to 12.90 ppb ppm^{-1}, indicating different emission sources in these areas. The ratio measured in the inner ring was a more accurate representation of the landfill emission ratio.

Natural gas filling stations are potential CH_4 emission sources, but no significant hotspots were detected near them. Figure 6 shows the correlation between ΔCH_4 and ΔCO_2 near two gas filling stations (Station 1: Sinopec Gas Station, on the southern side of Route 1; Station 2: Hangzhou Gas Filling Station, on the southern side of Route 4). At Station 1 (Fig. 6a), there were 26 passes during the day and 18 passes at night. The median ΔCH_4 value, the median ΔCO_2 value and the ratio in the inner ring were −50 ppb, 30.8 ppm, and 5.56 ppb ppm^{-1}, respectively. The corresponding values in the outer ring were −34 ppb, 35.7 ppm, and 5.61 ppb ppm^{-1}. For Station 2 (Fig. 6b), there were 27 passes during the day and 18 passes at night. The median ΔCH_4 value, the median ΔCO_2 value, and the ratio in the inner ring were −41 ppb, 21.9 ppm, and 3.29 ppb ppm^{-1}, respectively, whereas the median ΔCH_4 value, the median ΔCO_2 value, and the ratio in the outer ring were −50 ppb, 27.1 ppm, and 2.94 ppb ppm^{-1}. Both stations presented negative ΔCH_4 values (CH_4 concentrations lower than those at the reference station), with no significant difference between the inner ring and the outer ring. Compared with open streets, the ratio at Station 2 was close to that in the daytime on open streets (2.43 ppb ppm^{-1}), and the ratio at Station 1 was close to that in the nighttime (4.60 ppb ppm^{-1}), with no significant increase. These comparisons suggest that there was no natural gas leakage at these stations.

3.3. *Spatial patterns of ΔCH_4 and ΔCO_2 in various functional areas*

The ΔCH_4 values varied significantly across urban functional areas (Fig. 7a). During the day, the median ΔCH_4 values were ranked as follows: natural scenic area (49 ppb) > industrial area (40 ppb) > commercial–residential mixed area (22 ppb) > riverside residential area (2 ppb). The differences between most functional areas were statistically significant ($p < 0.05$), with the exception being between the natural scenic area and the industrial areas ($p > 0.05$). At night, the order was as follows: commercial–residential mixed area (94 ppb) > industrial area (79 ppb) > natural scenic area (59 ppb) > riverside residential area (5 ppb). There was no significant difference between the commercial–residential mixed area and the natural scenic area ($p > 0.05$). However, significant differences were detected between the other functional areas ($p < 0.05$).

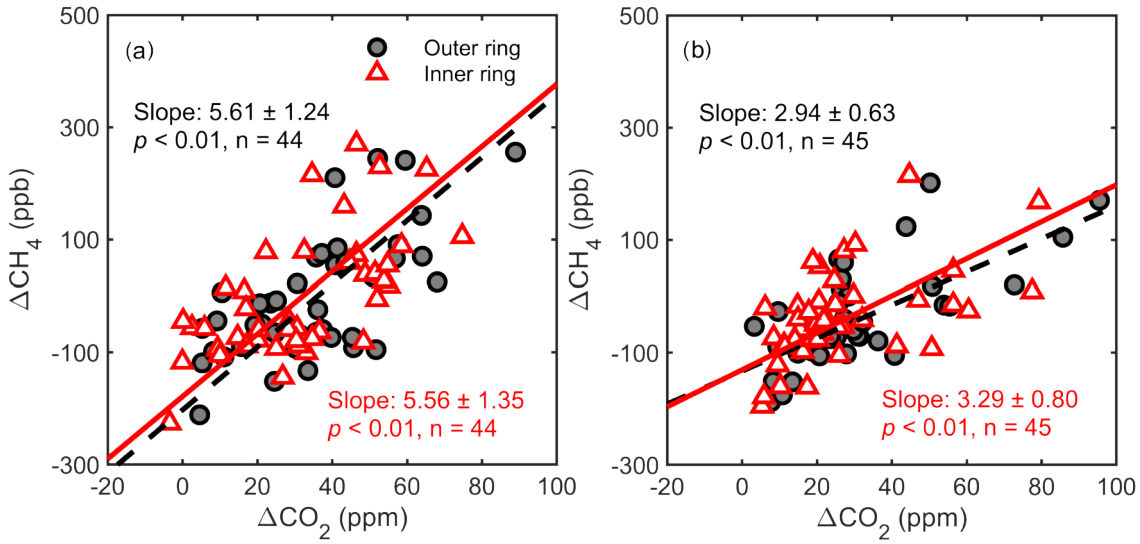

Fig. 6. Scatter plot of ΔCH_4 and ΔCO_2 detected near two gas filling stations: (a) Station 1 (Sinopec Gas Filling Station); (b) Station 2 (Hangzhou Gas Filling Station). Observations in the inner ring are denoted by open triangles, and those in the outer ring are denoted by solid circles. Lines indicate linear regression with statistics noted (slope value ± 95% confidence bounds).

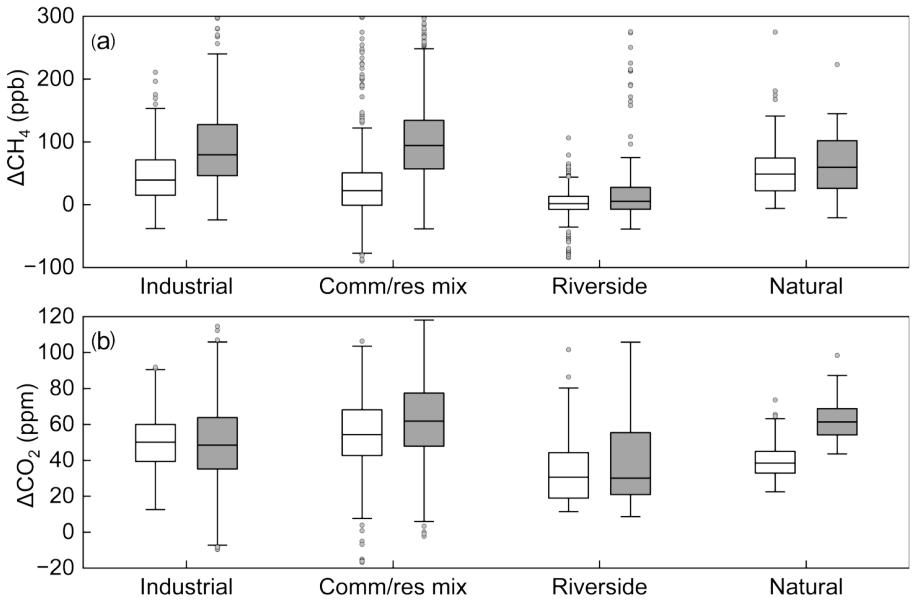

Fig. 7. The (a) ΔCH_4 and (b) ΔCO_2 for each functional area. The open boxes represent the daytime data, and the shaded boxes represent the nighttime data, including the median (line), 25th and 75th percentiles (box), 5th and 95th percentiles (whisker), and outliers (gray dots).

For ΔCO_2, the daytime median values were ranked as follows: commercial–residential mixed area (54.3 ppm) > industrial area (48.6 ppm) > natural scenic area (38.4 ppm) > riverside residential area (30.6 ppm), with significant differences between the areas ($p < 0.05$). At night, the order shifted as follows: commercial–residential mixed area (61.8 ppm) > natural scenic area (61.4 ppm) > industrial area (48.5 ppm) > riverside residential area (30.1 ppm). No significant difference was detected between the commercial–residential mixed area and the natural scenic area ($p > 0.05$), but other areas presented significant differences ($p < 0.05$). The median value of ΔCH_4 was greater at night than during the daytime in all the functional areas. These temporal and spatial patterns were consistent with the data shown in Fig. 2.

Affected by varying emission source types, the emission ratios differed across these functional areas (Fig. 8). During the day, negative ratios were obtained for the industrial area (−2.73 ppb ppm^{-1}) and the natural scenic area (−4.86 ppb ppm^{-1}), whereas positive ratios were recorded in the commercial–residential mixed area (3.34 ppb ppm^{-1}) and the riverside residential area (1.81 ppb ppm^{-1}). At night, all functional areas had positive slopes or emission ratios, with the industrial area having the highest ratio (13.01 ppb ppm^{-1}), followed by the riverside residential area (10.51 ppb ppm^{-1}), the natural scenic area (5.39 ppb ppm^{-1}), and the commercial–residential mixed area (3.36 ppb ppm^{-1}). The negative emission ratios were a result of photosynthesis by urban vegetation. Photosynthesis reduces the CO_2 concentration but does not affect the CH_4 concentration.

3.4. *CH_4 and CO_2 concentrations and emission ratios for traffic tunnels*

During the study, the measurement vehicles passed through the tunnels a total of 159 times during the day and 115 times at night. Figure S5 shows the corresponding concentrations. The median concentration of CH_4 was 2273 ppb during the day and 2379 ppb at night, indicating increases of 44 ppb during the day and 91 ppb at night compared with open street levels. For CO_2, the median concentrations were 554.1 ppm during the day and 560.4 ppm at night, revealing increases of 60.9 ppm and 42.4 ppm, respectively, compared with open street measurements.

Figure 9 shows the distribution of the CH_4:CO_2 emission ratios. During the day, the highest ratio was 9.19 ppb ppm^{-1}, the lowest ratio was −15.74 ppb ppm^{-1}, and the median ratio was 0.40 ppb ppm^{-1}. At night, the ratios ranged from −25.30 to 64.61 ppb ppm^{-1}, with a median ratio of 0.81 ppb ppm^{-1}. The nighttime ratios exhibited greater variation than those the daytime ratios did, and the median ratio at night was approximately twice that of the daytime value. By removing the top 5% and the bottom 5% of the extreme values, we obtain a mean emission ratio of 0.70 ± 1.11 ppb ppm^{-1} in the daytime, 1.48 ± 3.58 at night, and an overall ratio of 1.01 ± 1.82 ppb ppm^{-1}.

4. Discussion

4.1. *Emission hotspots*

This study employed a new method to identify emission hotspots. Chamberlain et al. (2016) identified hotspots in New York City (USA) using a threshold CH_4 concentration exceedance of 1.93 ppm. In Koch et al. (2016), a threshold of 2.5 ppm was used for CH_4 hotspots in Bryan and College Station, Texas, USA. Other studies have used mean concentrations and background values during experiments to classify

values 5%–10% greater than background levels as hotspots (Weller et al., 2018; Kohler et al., 2022). Although these methods are efficient at locating hotspots, they risk misjudgment at times of fluctuating background concentrations. Fur-

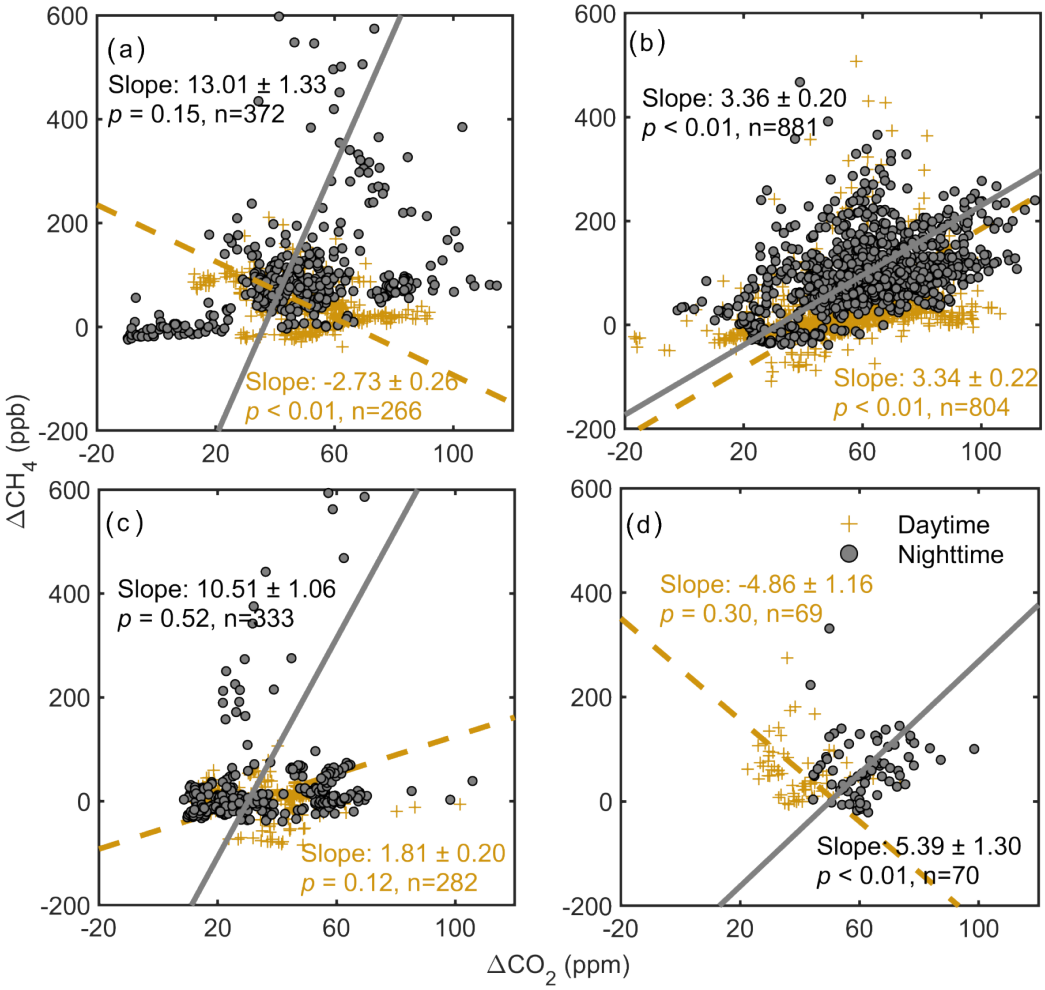

Fig. 8. Scatter plot of ΔCH_4 and ΔCO_2 for each functional area: (a) industrial area; (b) commercial–residential mixed area; (c) riverside residential area; and (d) natural scenic area. The data points represent observations. Lines indicate linear regression with statistics noted (slope value ± 95% confidence bounds).

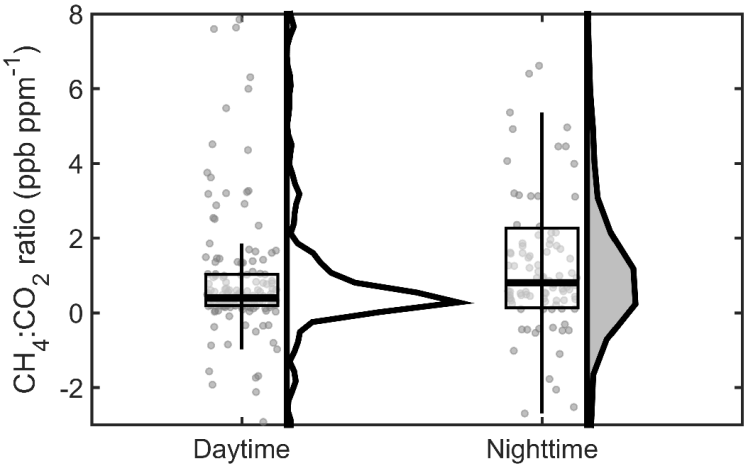

Fig. 9. Daytime and nighttime CH_4:CO_2 ratios in tunnels, showing the median (lines), 25% and 75% percentiles (boxes), 5th and 95th percentiles (whiskers), and frequency distributions (curves).

thermore, for sporadic emission sources, such as high-emission vehicles near sampling points, multiple measurements along the same route are needed to determine stable emission sources and reduce the likelihood of misclassification. This study accounted for both reference concentration fluctuations and occasional emissions by using enhancement values to emphasize the effects of local emissions. In addition, hotspots were defined on the basis of multiple appearances, ensuring the reliability of the identified sources.

The CH_4 and CO_2 hotspots identified in this study did not overlap completely. When it passes through a CH_4 hotspot, the ΔCH_4 concentration typically increases sharply, forming an "L" shape in the ΔCH_4 versus ΔCO_2 scatter plot. Urban infrastructure, such as landfills and sewage treatment plants, is a typical emission hotspot (Takano and Ueyama, 2021; Hu et al., 2023). In Hangzhou, a primary anthropogenic CH_4 emission source is waste management facilities (Hu et al., 2023). Even after closure, landfills can continue emitting large amounts of CH_4. In contrast, urban CO_2 hotspots are typically associated with vehicular emissions. High CO_2 concentrations tend to occur in areas with dense traffic and during specific traffic conditions, such as at intersections. Poor diffusion conditions, such as those created by sound insulation boards along elevated roads or densely built residential areas, can also create CO_2 hotspots.

The daily variation in CH_4 and CO_2 hotspots was significant, with ΔCH_4 and ΔCO_2 values generally greater at night than during the day. Two main factors likely explain this pattern: (1) Hangzhou enforced strict vehicle restrictions during the day, limiting the movement of nonlocal vehicles, particularly large trucks, which are permitted to enter the city only after 1900 LST (Hangzhou Traffic Police, 2023). (2) Hangzhou's nighttime economy has been expanding, with the construction of natural gas pipelines for outdoor food vendors contributing to higher nighttime emissions. These developments likely contributed to the increase in nighttime CH_4 and CO_2 concentrations. Hangzhou's efforts to promote all-night dining and entertainment might further intensify this day–night emission disparity.

4.2. *CH_4:CO_2 emissions ratio*

The seasonal variation in the CH_4:CO_2 ratio on open streets was weak, with slightly greater values in the summer and the autumn than in the spring and the winter. This variation is jointly affected by the emission sources of CH_4 and CO_2. Although the average ΔCH_4 levels in the spring and the winter were relatively high, the corresponding ΔCO_2 levels were also elevated. In contrast, increased photosynthetic activity during the summer and the autumn yielded a lower ΔCO_2 (the vegetation coverage in Hangzhou is 65%; https://www.hangzhou.gov.cn), resulting in a slightly increased CH_4:CO_2 ratio.

Table S1 in the ESM provides a summary of the CH_4:CO_2 emission ratios for several source types. The traffic emissions ratio was based on the data collected in traffic tunnels (Fig. 9). The sewage treatment emission ratio was based on the data collected near the Qige Sewage Treatment Plant in the riverside residential area (Fig. 5a); this treatment plant was selected because it is far from street traffic. The emissions ratio for the landfill was based on the data in Fig. 5b. The overall emissions ratio was based on data collected from open streets across the whole city (Fig. 1). The daily average traffic emissions ratio (1.01 ppb ppm^{-1}) is nearly identical to the IPCC default emissions ratio for gasoline vehicles (0.99 ppb ppm^{-1}; Stocker et al., 2013; Hu et al., 2018).

In studies of landfill emissions, the CH_4:CO_2 emissions ratio is highly variable, depending on landfill age, landfill content, and management regime. A survey of flux chamber observations revealed a mean emissions ratio of approximately 1200 ppb ppm^{-1}, with a standard deviation of 1670 ppb ppm^{-1} (Jha et al., 2008; Pandey et al., 2014; Popiţa et al., 2015; Gollapalli and Kota, 2018; Haro et al., 2019; Yilmaz et al., 2021; Dwivedi et al., 2022; Ikpe et al., 2023). Landfills release approximately one CH_4 molecule for every CO_2 molecule emitted. The emissions ratio that we measured (36.5 ppb ppm^{-1}) was only approximately 3% of this typical value. In previous chamber-flux studies, flux ratio observations were made inside landfills. In this study, observations were conducted outside the landfill. The emissions plume from the landfill was diluted by mixing with plumes from traffic sources with a much lower CH_4 content. This mixing may have biased the emissions ratio towards lower values. This landfill may have had a lower emissions ratio because of its age (33 years) and low organic content of solid waste. A low emissions ratio (35.11 ppb ppm^{-1}) has also been reported for landfills in a municipal solid waste landfill in the midwestern United States (Yilmaz et al., 2021).

Compared with the landfill emissions ratio, we are more confident about the emissions ratio for the sewage treatment plant. This occurred because (a) the plant was far from major traffic roads, (b) the correlation between CH_4 and CO_2 concentrations was highly significant, and (c) the emissions ratio was unaffected by expanding the measurement distance from the plant (Fig. 5a). To the best of our knowledge, no published studies have performed in situ measurements of the CH_4:CO_2 emissions ratio for sewage treatment plants. According to inventory data, this ratio is dependent on the treatment technology and varies from 3.4 ppb ppm^{-1} (activated sludge) to 1.45 ppm ppm^{-1} (anaerobic reactor; Wang et al., 2022). The emission ratios of these wastewater treatment methods vary widely. The emissions ratio in our study (12.76 ppb ppm^{-1}) was near the lower end of the reported range. This plant treats sewage with a combination of an improved anaerobic–anoxic–oxic process(AAO), denitrification deep bed filters, and ultraviolet disinfection.

The overall emissions ratio (3.46 ppb ppm^{-1}) was three times greater than the traffic emissions ratio (1.01 ppb ppm^{-1}) in Hangzhou, suggesting that in addition to traffic, other area sources contributed to the urban methane budget. One potential contributor is household consumption of natural gas. In a recent observational study of CH_4 emissions from

residential gas stoves and tankless water heaters in China, the mean emission factor was approximately 1.1 g CH_4 m^{-3} or 68.8 mmol CH_4 L^{-1} (Sun et al., 2024). Combining this estimate with the IPCC CO_2 emission factor of 43.9 mmol CO_2 L^{-1} from natural gas (Hu et al., 2018) yields an emissions ratio of 1.57 ppb ppm^{-1} for this residential source type. Because this ratio is actually smaller than the emissions ratio measured in open streets, this residential source was likely a negligible source of urban CH_4. On the other hand, waste treatment may be an important source. For the sake of augmentation, let us assume that the street-level concentrations were dominated by emissions from vehicle traffic and from sewage treatment plants and omit other source types. Using a two-source mixing model similar to Eq. (1), we estimate that sewage treatment was responsible for approximately 20% of the CH_4 emissions in Hangzhou. For a comparison, using CH_4 concentration data and backward trajectory modeling, Hu et al. (2023) estimated that waste treatment in Hangzhou released 5.5 $\times 10^4$ t CH_4 into the atmosphere in 2021, or approximately half of the total anthropogenic emissions. This proportion is greater than our simple two-source model estimate. In their study, waste treatment consisted of sewage treatment as well as other forms of waste disposal.

The emission source composition in each functional area clearly exhibited temporal variations. The CH_4:CO_2 ratios provided further insights into these patterns. For example, in industrial areas, the negative daytime ratio (caused by a sharp increase in ΔCH_4; Fig. 7a) shifted to a positive ratio at night. The commercial–residential mixed areas presented positive ratios during both day and night, suggesting that both vehicle emissions and natural gas stove emissions were significant sources. In addition, CH_4 emissions from vehicles, which can account for up to 30% of total emissions in heavy traffic areas (Nakagawa et al., 2005), likely play a significant role in these areas. In the natural scenic area, the negative daytime ratio was likely attributable to the effect of vegetation. Natural scenic areas act as CH_4 sources and CO_2 sinks (Huang et al., 2019; Sun et al., 2019). At night, vegetation shifts from a CO_2 sink to a source, explaining the positive ratio. In the residential area along the river, the ratio increased sharply at night because of emissions from the sewage treatment plant and nearby viaducts. These results suggest that vehicle emissions and sewage treatment plants were the primary contributors to emissions in this area.

4.3. *Vehicle fuel types*

The CH_4:CO_2 emission ratios for gasoline and natural gas vehicles differ significantly. Our overall emissions ratio of 3.46 ppb ppm^{-1}, measured in Hangzhou from 2020 to 2023, was only 30% of the emissions ratio reported for Nanjing in 2016 [12.3 ppb ppm^{-1}; Supplementary Table 2 in Hu et al. (2018)]. The result for Nanjing was also obtained via mobile measurements in open streets. Hu et al. (2018) used the same instrument as in this study. The main difference is the way the emissions ratio was calculated. In this study, the emissions ratio was calculated using enhancement values, whereas in the study on Nanjing, the emissions ratio was calculated using actual concentration data that included background concentrations. We also calculated the overall emissions ratio using the actual concentration data. The result was 3.70 ± 4.07 ppb ppm^{-1}, which was only 30% of the emission ratio reported for Nanjing. Both Hangzhou and Nanjing are located in the Yangtze River Delta and have similar urban infrastructures and fuel use mixtures. It is reasonable to assume that the difference was caused by a shift in fuel type in the transportation sector—specifically, a reduction in the fraction of natural gas vehicles. The mean traffic emissions ratio, which is based on data collected in traffic tunnels in Nanjing, was 2.7 ppb ppm^{-1} in 2016 (Supplementary Table 2 in Hu et al., 2018), which is nearly four times and twice the traffic emissions ratio obtained for Hangzhou during the day and at night (Table S1 in the ESM), respectively.

The data collected in tunnels can be used in a two-source mixing model to estimate vehicle compositions. The emissions ratio for natural gas vehicles is 31 ppb ppm^{-1} according to field observations in eight cities in China (Hu et al., 2018). Combining this number with the IPCC emission ratio for gasoline vehicles (0.99 ppb ppm^{-1}) and Eq. (1), we estimate that 99.93%, or nearly all nonelectric vehicles in Hangzhou, were gasoline-powered. The methodology established here is applicable to cities elsewhere.

Government policies have had a significant effect on vehicle fuel types in Chinese cities. Hangzhou city's "oil-to-gas" initiative, which was implemented in 2013, incentivized taxi operators to convert to natural gas, resulting in a high proportion of natural gas-fueled taxis in the years that followed. In more recent years, a new transition has occurred, as more vehicles have become electric (Zhejiang Provincial Department of Transportation, 2021). Further reductions in the use of natural gas-fueled taxis and buses are expected as electric vehicles become more common. Private vehicles, which comprise a significant portion of Hangzhou's vehicle fleet, have been slower in adopting natural gas because of the limited availability of refueling stations and the inconvenience of vehicle modifications. However, with the rapid development of electric vehicle infrastructure, more residents are opting for electric cars, which have no tailpipe emissions. This shift is expected to further reduce the proportion of gasoline and natural gas vehicles in cities.

4.4. *Roles of wetlands and water bodies*

The observational area in this study was confined to the main urban districts of Hangzhou, and the majority of the measurement routes were far from rivers or lakes. In the natural scenic area and riverside residential area, no significant CH_4 emission hotspots were identified. The median ΔCH_4 values obtained for these two functional areas were 49 ppb and 2 ppb during the daytime and 59 ppb and 5 ppb at night, respectively. Qin et al. (2016) reported that the CH_4 emissions flux in the Xixi wetland (one of the most important wetlands in Hangzhou) ranged from −0.0019 to 0.0353 mg m^{-2} h^{-1}. We are not aware of CH_4 flux data for rivers and lakes in cities. The CH_4 flux of the hypereutrophic Lake Taihu, approximately 150 km from Hangzhou, is approximately

0.2 mg m^{-2} h^{-1} (Xiao et al., 2014). Lakes and rivers in Hangzhou have much better water quality than Lake Taihu does, so their CH_4 flux should be lower than the Lake Taihu value. In comparison, the urban anthropogenic CH_4 flux was one to two orders of magnitude greater than the flux values reported by these authors. According to the EDGAR v6.0 inventory, urban anthropogenic sources in Hangzhou emit 14.5×10^4 t CH_4 annually, mostly in the urban core, with an area of 8.3×10^3 km^2 (Hu et al., 2023), which is equivalent to a flux density of 2.0 mg m^{-2} h^{-1}. Compared with those of urban anthropogenic CH_4 sources, the contributions of rivers and lakes to atmospheric CH_4 in the study area appear to be limited.

5. Conclusions

This research was carried out in Hangzhou city. The key findings of this study are summarized as follows:

(1) Temporal and spatial patterns: There were significant diurnal variations in CO_2 and CH_4 concentrations, with marked differences detected across different functional areas.

(2) Emission hotspots: CO_2 hotspots were located at elevated road intersections and expressways, whereas CH_4 hotspots were detected near sewage plants, landfills and some elevated bridge intersections. There was no evidence that the natural gas filling stations were CH_4 emission hotspots.

(3) Emission ratios: The CH_4:CO_2 emissions ratio (36.50 ± 10.15 ppb ppm^{-1}) obtained for the Tianziling Landfill was much lower than the typical ratio (1200 ppb ppm^{-1}) for landfills. The emissions ratio at the Qige Sewage Treatment Plant (12.76 ± 2.50 ppb ppm^{-1}) was near the low end of the emissions ratio for sewage treatment (3.4 ppb ppm^{-1} to 1.45 ppm ppm^{-1}).

(4) Traffic emissions: The low traffic emissions ratio (0.70 ppb ppm^{-1} during the day and 1.48 ppb ppm^{-1} at night) indicated the negligible role of natural gas vehicles in traffic CH_4 emissions. This result confirms that the recent displacement of natural gas vehicles by electric vehicles has had a detectable effect on atmospheric CO_2 and CH_4.

Traffic is a well-known source of urban CH_4. Our finding that waste treatment is another major source of CH_4 in Hangzhou is not new (Hu et al., 2023). The low emission ratios obtained for the landfill and the sewage treatment plant are new. Using atmospheric CH_4 concentrations to constrain an atmospheric inversion model, Hu et al. (2023) reported that the EDGAR inventory overestimated the emissions of waste treatment in Hangzhou by 90%. It is possible that the total emissions of this source category would decrease even further if the inversion model was additionally constrained by the emission ratios that we obtained.

Acknowledgements. This work was supported by the National Natural Science Foundation of China (Grant Nos. U24A20590, 42021004); the Joint funds of the Zhejiang Provincial Natural Science Foundation of China (Grant No. LZJMZ23D050002); the 333 Project of Jiangsu Province (Grant No. BRA2022023); the Natural Science Foundation of Jiangsu Province for Distinguished Young Scholars (Grant No. BK20220055); and the Key Laboratory of Ecosystem Carbon Source and Sink, China Meteorological Administration (Grant No. ECSS-CMA202302).

Electronic supplementary material. Supplementary material is available in the online version of this article at https://doi.org/10.1007/s00376-025-5059-4.

Data availability statement. The datasets used and/or analyzed during the current study are available from the corresponding author upon request.

Competing interests. The authors declare that they have no known competing financial interests or personal relationships that could have appeared to influence the work reported in this paper.

REFERENCES

Ahn, D. Y., D. L. Goldberg, T. Coombes, G. Kleiman, and S. C. Anenberg, 2023: CO_2 emissions from C40 cities: Citywide emission inventories and comparisons with global gridded emission datasets. *Environmental Research Letters*, **18**(3), 034032, https://doi.org/10.1088/1748-9326/acbb91.

Bush, S. E., F. M. Hopkins, J. T. Randerson, C. T. Lai, and J. R. Ehleringer, 2015: Design and application of a mobile ground-based observatory for continuous measurements of atmospheric trace gas and criteria pollutant species. *Atmospheric Measurement Techniques*, **8**(8), 3481–3492, https://doi.org/10.5194/amt-8-3481-2015.

Cai, B. F., C. Cui, D. Zhang, L. B. Cao, P. C. Wu, L. Y. Pang, J. H. Zhang, and C. Y. Dai, 2019: China city-level greenhouse gas emissions inventory in 2015 and uncertainty analysis. *Applied Energy*, **253**, 113579, https://doi.org/10.1016/j.apenergy.2019.113579.

Chamberlain, S. D., A. R. Ingraffea, and J. P. Sparks, 2016: Sourcing methane and carbon dioxide emissions from a small city: Influence of natural gas leakage and combustion. *Environmental Pollution*, **218**, 102–110, https://doi.org/10.1016/j.envpol.2016.08.036.

Chen, J. D., M. Gao, S. L. Cheng, X. Liu, W. X. Hou, M. L. Song, D. Li, and W. Fan, 2021: China's city-level carbon emissions during 1992–2017 based on the inter-calibration of nighttime light data. *Scientific Reports*, **11**, 3323, https://doi.org/10.1038/s41598-021-81754-y.

Ciais, P., P. Rayner, F. Chevallier, P. Bousquet, M. Logan, P. Peylin, and M. Ramonet, 2010: Atmospheric inversions for estimating CO_2 fluxes: Methods and perspectives. *Climatic Change*, **103**, 69–92, https://doi.org/10.1007/s10584-010-9909-3.

Clairotte, M., R. Suarez-Bertoa, A. A. Zardini, B. Giechaskiel, J. Pavlovic, V. Valverde, B. Ciuffo, and C. Astorga, 2020: Exhaust emission factors of greenhouse gases (GHGs) from European road vehicles. *Environmental Sciences Europe*, **32**, 125, https://doi.org/10.1186/s12302-020-00407-5.

Crippa, M., and Coauthors, 2020: High resolution temporal profiles in the Emissions Database for Global Atmospheric Research. *Scientific Data*, **7**, 121, https://doi.org/10.1038/

s41597-020-0462-2.

Cui, X. G., and Coauthors, 2019: Atmospheric observation-based estimation of fossil fuel CO_2 emissions from regions of central and southern California. *Science of the Total Environment*, **664**, 381–391, https://doi.org/10.1016/j.scitotenv.2019.01.081.

Duren, R. M., and C. E. Miller, 2012: Measuring the carbon emissions of megacities. *Nature Climate Change*, **2**, 560–562, https://doi.org/10.1038/nclimate1629.

Dwivedi, P., D. S. Rathore, and P. Gothalkar, 2022: A Determination of gas outflow fluxes and study its transport mechanism by the application of flux chamber technique from the two landfill sites of semiarid region of Rajasthan. *EQA-International Journal of Environmental Quality*, **50**, 26–38, https://doi.org/10.6092/issn.2281-4485/14953.

Fang, S. X., R. G. Du, B. Qi, Q. L. Ma, G. Z. Zhang, B. J. Chen, and J. Y. Li, 2022: Variation of carbon dioxide mole fraction at a typical urban area in the Yangtze River Delta, China. *Atmospheric Research*, **265**(3), 105884, https://doi.org/10.1016/j.atmosres.2021.105884.

Gollapalli, M., and S. H. Kota, 2018: Methane emissions from a landfill in north-east India: Performance of various landfill gas emission models. *Environmental Pollution*, **234**, 174–180, https://doi.org/10.1016/j.envpol.2017.11.064.

Gong, P., and Coauthors, 2019: Stable classification with limited sample: Transferring a 30-m resolution sample set collected in 2015 to mapping 10-m resolution global land cover in 2017. *Science Bulletin*, **64**(6), 370–373, https://doi.org/10.1016/j.scib.2019.03.002.

Han, P. F., and Coauthors, 2020: Evaluating China's fossil-fuel CO_2 emissions from a comprehensive dataset of nine inventories. *Atmospheric Chemistry and Physics*, **20**(19), 11 371–11 385, https://doi.org/10.5194/acp-20-11371-2020.

Hangzhou Bureau of Planning and Natural Resources, 2020: General Plan of land use in Hangzhou (2006 – 2020). [Availableonline from http://ghzy.hangzhou.gov.cn/art/2020/1/9/art_1228962782_41563990.html]. (in Chinese)

Hangzhou Bureau of Statistics, 2020: Hangzhou Statistical Yearbook 2020. [Available online from https://tjj.hangzhou.gov.cn/art/2020/10/29/art_1229453592_3819709.html]. (in Chinese)

Hangzhou Traffic Police, 2023: Notice on Optimizing and Adjusting Traffic Management Measures for Certain Freight Vehicles in the Main Urban Area. [Available online from https://www.hzzx.gov.cn/cshz/content/2023-05/17/content_8535850.htm] (in Chinese)

Haro, K., and Coauthors, 2019: Assessment of CH_4 and CO_2 surface emissions from Polesgo's landfill (Ouagadougou, Burkina Faso) based on static chamber method. *Advances in Climate Change Research*, **10**(3), 181–191, https://doi.org/10.1016/j.accre.2019.09.002.

Hsu, Y.-K., T. VanCuren, S. Park, C. Jakober, J. Herner, M. FitzGibbon, D. R. Blake, and D. D. Parrish, 2010: Methane emissions inventory verification in southern California. *Atmos. Environ.*, **44**(1), 1–7, https://doi.org/10.1016/j.atmosenv.2009.10.002.

Hu, C., and Coauthors, 2023: Global warming will largely increase waste treatment CH_4 emissions in Chinese megacities: Insight from the first city-scale CH_4 concentration observation network in Hangzhou, China. *Atmospheric Chemistry and Physics*, **23**(7), 4501–4520, https://doi.org/10.5194/acp-23-4501-2023.

Hu, N., S. D. Liu, Y. Q. Gao, J. P. Xu, X. Zhang, Z. Zhang, and X. Lee, 2018: Large methane emissions from natural gas vehicles in Chinese cities. *Atmos. Environ.*, **187**, 374–380, https://doi.org/10.1016/j.atmosenv.2018.06.007.

Huang, W. J., and Coauthors, 2019: Anthropogenic CH_4 emissions in the Yangtze River Delta based on a "top-down" method. *Atmosphere*, **10**(4), 185, https://doi.org/10.3390/atmos10040185.

Huang, W. J., T. J. Griffis, C. Hu, W. Xiao, and X. Lee, 2021: Seasonal variations of CH_4 emissions in the Yangtze River Delta region of China are driven by agricultural activities. *Adv. Atmos. Sci.*, **38**(9), 1537–1551, https://doi.org/10.1007/s00376-021-0383-9.

Ikpe, E. A., N. E. Akpan, and M. O. Bassey, 2023: Design and construction of an energy specific landfill gas production system for use in Nigeria. *Advances in Engineering Design Technology*, **5**(1), 13–28, https://doi.org/10.5281/zenodo.7741915.

Janssens-Maenhout, G., and Coauthors, 2019: EDGAR v4.3.2 Global Atlas of the three major greenhouse gas emissions for the period 1970–2012. *Earth System Science Data*, **11**(3), 959–1002, https://doi.org/10.5194/essd-11-959-2019.

Jha, A. K., C. Sharma, N. Singh, R. Ramesh, R. Purvaja, and P. K. Gupta, 2008: Greenhouse gas emissions from municipal solid waste management in Indian mega-cities: A case study of Chennai landfill sites. *Chemosphere*, **71**(4), 750–758, https://doi.org/10.1016/j.chemosphere.2007.10.024.

Joo, J., S. Jeong, J. Shin, and D. Y. Chang, 2024: Missing methane emissions from urban sewer networks. *Environmental Pollution*, **342**, 123101, https://doi.org/10.1016/j.envpol.2023.123101.

Koch, K., S. Thomas, E. Arana, G. Roest, and G. W. Schade, 2016: On methane leaks from pipelines in Bryan and College Station, Texas, USA. *The Open Atmospheric Science Journal*, **10**, 56–62, https://doi.org/10.2174/1874282301610010056.

Kohler, F. K., C. Schaller, and O. Klemm, 2022: Quantification of urban methane emissions: A combination of stationary with mobile measurements. *Atmosphere*, **13**(10), 1596, https://doi.org/10.3390/atmos13101596.

Lee, J. K., A. Christen, R. Ketler, and Z. Nesic, 2017: A mobile sensor network to map carbon dioxide emissions in urban environments. *Atmospheric Measurement Techniques*, **10**(2), 645–665, https://doi.org/10.5194/amt-10-645-2017.

Li, S. L., S. Kim, H. Lee, S. T. Kenea, J. E. Kim, C. Y. Chung, and Y.-H. Kim, 2022: Analysis of source distribution of high carbon monoxide events using airborne and surface observations in Korea. *Atmos. Environ.*, **289**, 119316, https://doi.org/10.1016/j.atmosenv.2022.119316.

Liu, D., and Coauthors, 2021: Observed decreases in on-road CO_2 concentrations in Beijing during COVID-19 restrictions. *Atmospheric Chemistry and Physics*, **21**, 4599–4614, https://doi.org/10.5194/acp-21-4599-2021.

Lopez-Coto, I., S. Ghosh, K. Prasad, and J. Whetstone, 2017: Tower-based greenhouse gas measurement network design—the national institute of standards and technology North East Corridor Testbed. *Adv. Atmos. Sci.*, **34**, 1095–1105, https://doi.org/10.1007/s00376-017-6094-6.

Marcotullio, P. J., A. Sarzynski, J. Albrecht, and N. Schulz, 2014: A top-down regional assessment of urban greenhouse gas emissions in Europe. *AMBIO*, **43**, 957–968, https://doi.org/10.1007/s13280-013-0467-6.

Mustafa, F., L. B. Bu, Q. Wang, N. Yao, M. Shahzaman, M.

Bilal, R. W. Aslam, and R. Iqbal, 2021: Neural-network-based estimation of regional-scale anthropogenic CO_2 emissions using an Orbiting Carbon Observatory-2 (OCO-2) dataset over East and West Asia. *Atmospheric Measurement Techniques*, **14**, 7277–7290, https://doi.org/10.5194/amt-14-7277-2021.

Nakagawa, F., and Coauthors, 2005: Automobile exhaust as a source of ^{13}C- and D-enriched atmospheric methane in urban areas. *Organic Geochemistry*, **36**, 727–738, https://doi.org/10.1016/j.orggeochem.2005.01.003.

Oda, T., and Coauthors, 2019: Errors and uncertainties in a gridded carbon dioxide emissions inventory. *Mitigation and Adaptation Strategies for Global Change*, **24**, 1007–1050, https://doi.org/10.1007/s11027-019-09877-2.

Pan, D., and Coauthors, 2020: Methane emissions from natural gas vehicles in China. *Nature Communications*, **11**, 4588, https://doi.org/10.1038/s41467-020-18141-0.

Pandey, J., P. Kaushik, M. Mehra, and S. Masood, 2014: Methane and carbon dioxide emission and leachate characterization from landfills along Ganges river at Varanasi (U.P.), India. *Plant Archives*, **14**(1), 7–13.

Popiţa, G.-E., and Coauthors, 2015: Evaluation of carbon dioxide and methane emission from Cluj-Napoca municipal landfill, Romania. *Environmental Engineering and Management Journal*, **14**(6), 1389–1398, https://doi.org/10.30638/eemj.2015.151.

Potere, D., and A. Schneider, 2007: A critical look at representations of urban areas in global maps. *GeoJournal*, **69**, 55–80, https://doi.org/10.1007/s10708-007-9102-z.

Qi, B., and Coauthors, 2025: Using urban-suburban difference of atmospheric CO_2 to evaluate carbon neutrality capacity in Hangzhou, China. *Journal of Environmental Sciences*, **157**, 908–923, https://doi.org/10.1016/j.jes.2024.10.027.

Qin, S., J. Tang, J. Pu, Y. Xu, P. Dong, L. Jiao, and J. Guo, 2016: Fluxes and influencing factors of CO_2, and CH_4 in Hangzhou Xixi wetland, China. *Earth and Environment*, **44**, 513–519,https://doi.org/10.14050/j.cnki.1672-9250.2016.05.005. (in Chinese with English abstract)

Seto, K. C., and Coauthors, 2014: Human settlements, infrastructure and spatial planning. *Climate Change 2014: Mitigation of Climate Change. Contribution of Working Group III to the Fifth Assessment Report of the Intergovernmental Panel on Climate Change*, Edenhofer et al., Eds., Cambridge University Press, Cambridge, United Kingdom and New York, NY, USA.

Shorter, J. H., and Coauthors, 1996: Methane emission measurements in urban areas in eastern Germany. *Journal of Atmospheric Chemistry*, **24**(2), 121–140, https://doi.org/10.1007/BF00162407.

Stocker, T. F., and Coauthors, 2013: *Climate Change 2013: The Physical Science Basis. Contribution of Working Group I to the Fifth Assessment Report of IPCC the Intergovernmental Panel on Climate Change*, Cambridge University Press, Cambridge, UK., 1535pp.

Sun, M. X., X. M. Huang, G. Y. Pan, J. Y. Wang, Y. B. Zhou, Y. L. Hu, and D. L. Xie, 2024: Measurement and quantification of methane emissions from residential gas stoves and tankless water heaters in China. *Urban Climate*, **56**, 101997, https://doi.org/10.1016/j.uclim.2024.101997.

Sun, W. Q., L. C. Deng, G. M. Wu, L. Wu, P. F. Han, Y. C. Miao, and B. Yao, 2019: Atmospheric monitoring of methane in Beijing using a mobile observatory. *Atmosphere*, **10**(9), 1–12, 554, https://doi.org/10.3390/atmos10090554.

Takano, T., and M. Ueyama, 2021: Spatial variations in daytime methane and carbon dioxide emissions in two urban landscapes, Sakai, Japan. *Urban Climate*, **36**, 100798, https://doi.org/10.1016/j.uclim.2021.100798.

Turner, A. J., A. A. Shusterman, B. C. McDonald, V. Teige, R. A. Harley, and R. C. Cohen, 2016: Network design for quantifying urban CO_2 emissions: Assessing trade-offs between precision and network density. *Atmospheric Chemistry and Physics*, **16**(21), 13 465–13 475, https://doi.org/10.5194/acp-16-13465-2016.

Wang, D., and Coauthors, 2022: Greenhouse gas emissions from municipal wastewater treatment facilities in China from 2006 to 2019. *Scientific Data*, **9**(1), 317, https://doi.org/10.1038/s41597-022-01439-7.

Wang, R., and Coauthors, 2013: High-resolution mapping of combustion processes and implications for CO_2 emissions. *Atmospheric Chemistry and Physics*, **13**(10), 5189–5203, https://doi.org/10.5194/acp-13-5189-2013.

Wei, C., and M. H. Wang, 2020: Spatial distribution of greenhouse gases (CO_2 and CH_4) on expressways in the megacity Shanghai, China. *Environmental Science and Pollution Research*, **27**(25), 31 143–31 152, https://doi.org/10.1007/s11356-020-09372-1.

Weller, Z. D., J. R. Roscioli, W. C. Daube, B. K. Lamb, T. W. Ferrara, P. E. Brewer, and J. C. von. Fischer, 2018: Vehicle-based methane surveys for finding natural gas leaks and estimating their size: Validation and uncertainty. *Environmental Science & Technology*, **50**(20), 11 922–11 930, https://doi.org/10.1021/acs.est.8b03135.

Wu, K., T. Lauvaux, K. J. Davis, A. J. Deng, I. L. Coto, K. R. Gurney, and R. Patarasuk, 2018: Joint inverse estimation of fossil fuel and biogenic CO_2 fluxes in an urban environment: An observing system simulation experiment to assess the impact of multiple uncertainties. *Elementa*: *Science of the Anthropocene*, **6**(1), 17, https://doi.org/10.1525/elementa.138.

Xiao, W., and Coauthors, 2014: A flux-gradient system for simultaneous measurement of the CH_4, CO_2, and H_2O fluxes at a lake-air interface. *Environ. Sci. Technol.*, **48**(24), 14 490–14 498, https://doi.org/10.1021/es5033713.

Xueref-Remy, I., C. Messager, D. Filippi, M. Pastel, P. Nedelec, M. Ramonet, J. D. Paris, and P. Ciais, 2011: Variability and budget of CO_2 in Europe: Analysis of the CAATER airborne campaigns-part 1: Observed variability. *Atmospheric Chemistry and Physics*, **11**(12), 5655–5672, https://doi.org/10.5194/acp-11-5655-2011.

Yilmaz, M., J. M. Tinjum, C. Acker, and B. Marten, 2021: Transport mechanisms and emission of landfill gas through various cover soil configurations in an MSW landfill using a static flux chamber technique. *Journal of Environmental Management*, **280**, 111677, https://doi.org/10.1016/j.jenvman.2020.111677.

Zhang, Z. Q., and Coauthors, 2024: Development of a regional carbon assimilation system and its application for estimating fossil fuel carbon emissions in the Yangtze River Delta, China. *Science of the Total Environment*, **957**, 177720, https://doi.org/10.1016/j.scitotenv.2024.177720.

Zhao, C. L., and P. P. Tans, 2006: Estimating uncertainty of the WMO mole fraction scale for carbon dioxide in air. *J. Geophys. Res.*: *Atmos.*, **111**(D8), D08S09, https://doi.org/10.1029/2005JD006003.